Second harmonic generation observed by dielectric relaxation at high electric fields: SHG without optics

Erik Thoms and Ranko Richert*

School of Molecular Sciences, Arizona State University, Tempe, Arizona 85287, USA

Abstract: We have measured second harmonic generation (SHG) via the nonlinear dielectric permittivity of a polar glass-forming liquid, propylene glycol, with the inversion symmetry of the liquid broken by applying a dc bias field. For a given combined peak field, $E_B + E_0$, highest second harmonic signals are obtained when the dc bias field and peak ac-field have the same amplitude, i.e., $E_B = E_0$. Second harmonic results measured in the static limit agree well with the theoretical prediction based upon the third-order nonlinear susceptibility term that connects polarization P with the static field E. Second harmonic signals are detectable at all frequencies at which dipole orientation contributes to permittivity, possibly occurring the instant a dc bias field is applied. The results imply that second harmonic generation as a signature of anisotropy, e.g., at interfaces, can be assessed by impedance spectroscopy at twice the fundamental frequency, not only by optical techniques.

Keywords: nonlinear dielectric effects, second harmonic generation, high electric fields, supercooled liquids.

Corresponding author e-mail: ranko@asu.edu

I. INTRODUCTION

Second harmonic generation (SHG) is the lowest order nonlinear effect of a medium, where the response to a sinusoidal force (e.g., an electromagnetic wave) at frequency ω contains contributions at 2ω. One of the most common and useful applications of SHG is the frequency doubling of laser light.[1] Even order nonlinear effects such as SHG will not occur in systems with inversion symmetry regarding a transition dipole moment or permanent dipole moment. Therefore, observing second harmonic signals in amorphous materials such as liquids, glasses, or polymers can be used to detect anisotropy, for instance as a result of spontaneous molecular alignment at an interface.[2] For materials with inversion symmetry in the bulk, SHG can thus be used as surface-specific measurement tool. Moreover, the inversion symmetry of an amorphous polymer can be broken by poling, the electric field induced orientation of molecular dipoles at temperatures above the segmental glass transition, which can then be preserved by cooling to the rigid glassy state. After poling, a bulk polymer sample can evoke frequency doubling of intense laser light.[3,4] This feature has been exploited to measure the decay of anisotropy in poled glassy polymers via the intensity of the light detected at 2ω, where ω is the frequency of the laser light. An advantageous feature of this technique is that the SHG intensity vanishes when the sample has reached the isotropic equilibrium state.

The polarization P of dielectric materials by an electric field E follows the same basic rules: susceptibilities χ_n of even order n vanish for materials with inversion symmetry.[5,6,7,8] In the context of liquids and supercooled liquids, the steady state polarization response of a material to high fields is commonly characterized by susceptibilities χ_n, so that $P(E)$ is expressed by

$$\varepsilon_0^{-1} P = \chi E + \chi_3 E^3 \,, \tag{1}$$

where ε_0 is the permittivity of vacuum ($\chi \equiv \chi_1$). Higher order terms (χ_5, χ_7, ...) are typically very small and thus disregarded here. As a result of the absence of χ_2 in Eq. (1), no second harmonic contributions to $P(t)$ are expected when applying a sinusoidal (ac) electric field $E(t) = E_0 \sin(\omega t)$. However, the inversion symmetry can be broken by applying a dc bias field E_B, which tilts the potential energy in the direction of the electric field E_B. Consequently, the superposition of an ac and a dc field is expected to give rise to a second harmonic polarization response.

This study differs from previous reports of SHG in that no optical detection is involved. Instead, the anisotropy responsible for SHG is detected via the nonlinear dielectric permittivity at 2ω. There has been considerable recent interest in nonlinear dielectric phenomena from both the experimental[9,10,11,12,13,14,15,16,17,18,19,20] and theoretical[21,22,23,24] perspective, but to our knowledge the

second harmonic permittivity has not been studied by experiment to date. The aim of this work is to outline how to measure a dielectric SHG signal, provide experimental results for the case of propylene glycol (PG), and test these results against theoretical expectations. We find that the optimal field pattern for such experiments is achieved with the condition $E_B = E_0$. The amplitude of the SHG signal is consistent with the known value of χ_3 for PG in the static limit, and diminishes following the real component of the relaxing part of permittivity, $\varepsilon'(\omega) - \varepsilon_\infty$, at elevated frequencies.

II. EXPERIMENT

The material propylene glycol (PG, >99.5%) has been obtained from Sigma-Aldrich and is used as received. For the parallel plate capacitor, the electrode separation d is defined by monodisperse silica microspheres with diameter 9.2 μm (Cospheric), mixed into an aliquot of PG to obtain a composition of order 100 ppm by volume. This mixture is filled into a spring-loaded capacitor cell with a pair of titanium electrodes with 17 mm and 20 mm diameter and a geometric capacitance of C_{geo} = 218 pF.[25] The cell is mounted onto the cold finger of an evacuated closed cycle He-refrigerator cryostat (Leybold RDK 6-320, Coolpak 6200), and its temperature is controlled by a Lakeshore Model 340 equipped with DT-470-CU diode sensors.

The applied electric field $E(t) = E_B + E_0 \sin(\omega t)$ is derived from an arbitrary waveform generator (Stanford Research Systems DS-345) after boosting its output by a factor of 100 via a high-voltage amplifier (Trek PZD-350), whose output is connected to the high-potential side (V_{hi}) of the sample capacitor. The low-potential side (V_{lo}) of the capacitor is connected to ground via a shunt with resistance R =1 kΩ or 100 Ω (50 W). Both potentials, V_{hi} and V_{lo}, are measured with a data acquisition unit (Nicolet Sigma 100) and yield the voltage across ($V = V_{hi} - V_{lo}$) and the current through ($I = V_{lo}/R$) the capacitor. The field protocol includes multiple zones with distinct E_B levels, shown schematically in Fig. 1 for the two different field patterns applied to measure nonlinear responses, but drawn with fewer cycles per zone than actually used, for clarity. Within each zone the ac and dc amplitudes are constant, and the frequency is unchanged for the entire duration of applying the field. To achieve a good signal to noise ratio, 5000 waveforms of $V(t)$ and $I(t)$ are averaged at a repetition rate of one per 1 - 4 seconds, with a field applied 10% of the total time at most. Signals are recorded at a resolution of 12 bit with at least 100 points per cycle of the fundamental frequency. To obtain results associated with the static limit, measurements are performed at frequencies sufficiently below the loss peak frequency ν_{max}. Each period with duration $2\pi/\omega$ of the $V(t)$ and $I(t)$ signals is then subjected to Fourier analysis, and the responses at frequency $n\omega$ are calculated via

$$\varepsilon'_{\mathrm{E,n}} = \frac{|I_\mathrm{n}|/|V_1|}{n\omega C_\mathrm{geo}} \sin\left(\varphi_{\mathrm{I_n}} - \varphi_{\mathrm{V_1}}\right), \tag{2a}$$

$$\varepsilon''_{\mathrm{E,n}} = \frac{|I_\mathrm{n}|/|V_1|}{n\omega C_\mathrm{geo}} \cos\left(\varphi_{\mathrm{I_n}} - \varphi_{\mathrm{V_1}}\right), \tag{2b}$$

using amplitudes ($|I_\mathrm{n}|, |V_1|$) and phases ($\varphi_{\mathrm{I_n}}, \varphi_{\mathrm{V_1}}$) of the applied voltage (V_1) and n^{th} harmonic of the current (I_n), as derived from the Fourier analysis. Note that high field permittivities, ε_E, are evaluated analogous to their low field (linear regime) counterpart, see Eq. (2). Details of the calculation can be found elsewhere.[26] Permittivities derived from impedance type measurements are denoted ε for low field and $\varepsilon_{\mathrm{E,n}}$ for high field results, as in Eq. (2), while the variables χ_n (with $\chi \equiv \chi_1$) are used only for the relation between P and E as in Eq. (1).

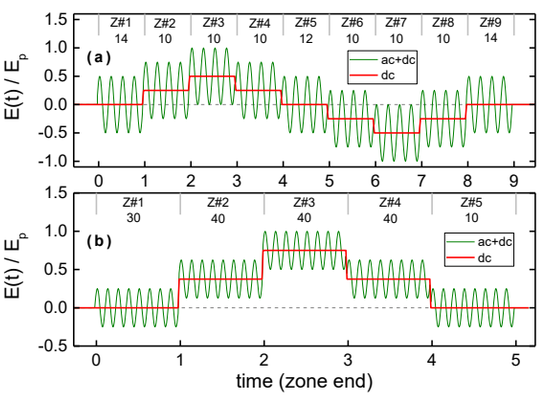

Fig. 1. Schematic representation of the field patterns (a) and (b) used in this study to measure the nonlinear responses, normalized to the peak field E_p of the entire pattern. (a) In each of the nine zones (numbered 1 to 9, see top legend) the dc bias field is either zero, $\pm E_\mathrm{p}/4$, or $\pm E_\mathrm{p}/2$ (see red levels), with ac amplitude $E_0 = E_\mathrm{p}/2$. (b) In each of the five zones (numbered 1 to 5, see top legend) the dc bias field is either zero, $\pm 3E_\mathrm{p}/8$, or $\pm 3E_\mathrm{p}/4$ (see red levels), with $E_0 = E_\mathrm{p}/4$. The ac-field component has a constant frequency ν and amplitude E_0 in all zones. The actual number of cycles per zone is indicated below the zone number.

Unavoidably, a signal generator together with the high voltage amplifier will have a finite offset bias voltage and some second harmonic contribution to the overall voltage output applied to the sample. The bias offset has been determined not to exceed 0.4% of the overall peak voltage E_p, and is thus negligible. The second harmonic contribution to the applied voltage was determined to have an amplitude $|V_2| \approx 10^{-3}|V_1|$ at $\nu = 5$ kHz, with only little dependence on the load and on the bias voltage V_B, but $|V_2|$ is reduced at lower frequencies. This may need to be accounted for when $|I_2| \approx 10^{-2}|I_1|$ or less. In the context of high alternating fields, sample heating is a common concern. The highest power level that occurred with the present experiments was $P = 0.18$ W. Assuming that the electrodes act as efficient heat sinks, the average temperature increase is $\Delta T_\mathrm{avg} = Pd^2/(12\kappa\upsilon)$. Using the power $P = 0.18$ W, thickness $d = 10$ µm, volume

$\upsilon = 2.4\times10^{-9}$ m^3, and thermal conductivity $\kappa = 0.2$ W m^{-1} K^{-1},[27] the average increase in temperature is $\Delta T_{avg} = 5$ mK, which is considered negligible.

III. RESULTS

Low field dielectric loss spectra versus frequency are depicted for PG in Fig. 2, emphasizing that ε'' at the temperature $T = 225$ K shows a minimum near the frequency of $\nu = 5$ kHz, the situation presently used for the high field experiments in the static limit. These data are taken from a previous measurement using the same material, cryostat, and temperature control unit,[26] and are consistent with results for the present samples and with previous reports.[28,29] Comparing the amplitudes of these bulk PG experiments with those obtained in the high field cell, it is found that the actual electrode separation of that cell is up to 15% higher than the nominal silica microsphere diameter of 9.2 μm. As has been shown by Bauer *et al.*,[30] such microspheres do not affect high field dielectric measurements adversely and do not lead to significant Maxwell-Wagner polarization.

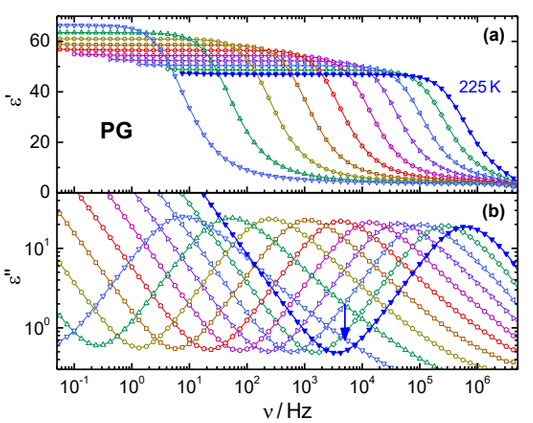

Fig. 2. Plot of ε' (a) and ε'' (b) versus frequency for PG at nominal temperatures from $T = 180$ to 225 K in steps of 5 K, measured in the low-field limit. The solid symbols represent spectra for $T = 225$ K, the temperature at which the present experiments in the static limit are performed. The frequency $\nu = 5$ kHz used for the high field experiments in the static limit is indicated by the arrow and selected to be near the loss minimum at $T = 225$ K. The data is taken from Ref. 26, where the same cell and cryostat had been used.

Regarding the choice for the E_B to E_0 ratio used to detect second harmonics, one might be tempted to use a high value of E_B to generate a large polarization anisotropy and a moderate ac level E_0 to measure second harmonic permittivities. However, the amplitude of $\varepsilon'_{E,2}$ is expected to be proportional to the product $E_B \times E_0$.[31] Therefore the optimal ratio for a given peak field $E_p = E_B + E_0$ is given by $E_B = E_0$, a condition that maximizes $E_B \times E_0$ and that has been used for the present experiments aimed at observing responses in the static limit. Results of measurements using the field pattern schematically represented in Fig. 1(a) are depicted as symbols in Fig. 3, which show the real part of the second harmonic dielectric

response, $\varepsilon'_{E,2}$, determined from $V_1(t)$ and $I_2(t)$ via Eq. (2) for each period of the $\nu = 5$ kHz field. The level of $\varepsilon'_{E,2}$ is practically time invariant within each zone (region of constant field amplitude E_B), because the dielectric relaxation is fast (characteristic relaxation time $\tau_{max} = 1/(2\pi\nu_{max}) = 0.27$ μs) compared to the duration of one period (200 μs) of the ac field with $\nu = 5$ kHz. This condition of $\nu << \nu_{max} = 6\times10^5$ Hz at $T = 225$ K guarantees that responses in the static limit are being observed.

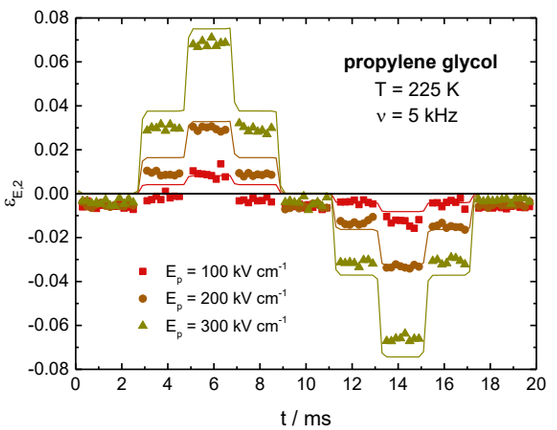

Fig. 3. Symbols represent results for the second harmonic high field permittivity in the static limit, $\varepsilon_{E,2}$, of PG at $T = 225$ K versus time. Values for each period of the $\nu = 5$ kHz field are derived from the Fourier analysis at twice the fundamental frequency, i.e., at $2\nu = 10$ kHz. The peak fields are $E_p = 300$ kV cm^{-1} (olive triangles), 200 kV cm^{-1} (brown circles), and 100 kV cm^{-1} (red squares), half of which is the peak ac field E_0. The dc bias is zero in zones 1, 5, and 9, $\pm E_p/4$ in zones 2, 4, 6, and 8, and $\pm E_p/2$ in zones 3 and 7. Lines reflect the levels expected based on the value of χ_3 for PG and Eq. (3b).

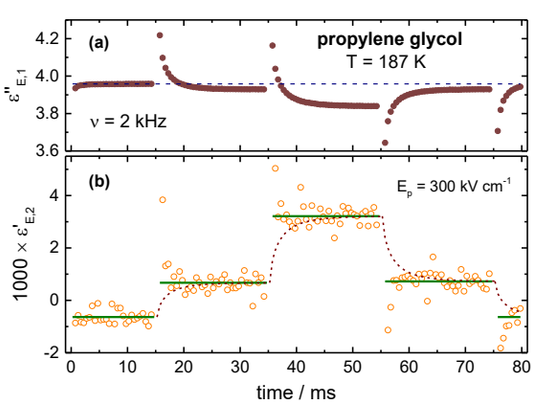

Fig. 4. Time resolved dielectric measurement of $\varepsilon''_{E,1}$ (a) and $\varepsilon'_{E,2}$ (b) at $\nu = 2$ kHz using the field pattern of Fig. 1(b). Results are for PG at $T = 187$ K, where the peak loss frequency is at $\nu_{max} = 74$ Hz. The dashed line in panel (a) indicates the level of $\varepsilon''_{E,1}$ in the absence of a dc bias field, the dashed curve in (b) reflects the low field α-relaxation response measured *in situ*. The green bars in (b) represent the average over data points in each zone. The $\varepsilon''_{E,1}$ curve indicates the time scale of structural recovery to the E_B steps, whereas the second harmonic signal $\varepsilon'_{E,2}$ appears to adjust faster than this α-relaxation (dashed line, stretched exponentials, $\exp[-(t/\tau_0)^{\beta}]$, with $\tau_0 = 1.8$ ms and $\beta = 0.7$).

A further experiment focuses on the second harmonic signal at a lower temperature $T = 187$ K with $\tau_{max} = 2.2$ ms and a frequency $\nu = 2$ kHz, i.e., above that of the loss peak at $\nu_{max} = 74$ Hz, using the five-

zone field pattern depicted in Fig. 1(b). The results of this measurement at $T = 187$ K are shown in Fig. 4, with $\varepsilon''_{E,1}$ indicating the time scale of structural recovery (τ_α) in response to the applied dc-field. Note that the rise above the $E_B = 0$ level (dashed line) originates from energy absorption, while the drop below that level reflects the field induced increase of τ_α.[15,16] This impact of E_B on the permittivity at the fundamental frequency (see $\varepsilon''_{E,1}$ in Fig. 4(a)) leads to the spikes of $\varepsilon'_{E,2}$ occurring with every step in E_B. Beyond these spikes, the second harmonic signal, $\varepsilon'_{E,2}$, is almost constant within each zone of constant E_B, and thus appears to reach steady state as least as fast as the dipole reorientation governing the α-relaxation, which is represented by the dashed curve in Fig. 4(b). The real part of permittivity at the test frequency of $\nu = 2$ kHz is about 5.6 and thus more than a factor of 10 below the static dielectric constant, $\varepsilon_s = 62$, at this temperature $T = 187$ K.

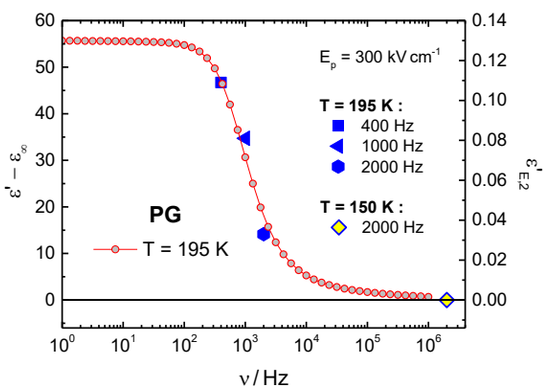

Fig. 5. Interconnected circles represent the low-field permittivity spectrum, $\varepsilon'(\omega) - \varepsilon_\infty$, for the same PG sample used to measure the nonlinear effects. The four larger symbols are for second harmonic results, $\varepsilon'_{E,2}(\omega)$ recorded with $E_p = 300$ kV cm^{-1} using the pattern of Fig. 1(b) and at frequencies between $\nu = 400$ to 2000 Hz, as indicated. All data are recorded at $T = 195$ K, with the exception of the case shown as diamond, for which $T = 150$ K was used. The frequency position of the diamond is arbitrarily set at $\nu = 2$ MHz, where $\varepsilon' \approx \varepsilon_\infty$, consistent with the rigid glassy state of PG at $\nu = 2$ kHz and $T = 150$ K (= $T_g - 18$ K).

In order to assess the frequency dependence of the second harmonic permittivity in more detail, nonlinear experiments have been performed at $T = 195$ K for frequencies 400, 1000, and 2000 Hz and using the field pattern of Fig. 1(b). These results are shown as zone-averaged values of $\varepsilon'_{E,2}$ in Fig. 5, demonstrating that the levels of $\varepsilon'_{E,2}(\omega)$ decline with increasing frequency proportional to the dipolar contribution to the real part of the low-field permittivity, $\varepsilon'(\omega) - \varepsilon_\infty$. Because the present equipment does not facilitate measurements at frequencies where $\varepsilon' \approx \varepsilon_\infty$ at $T = 195$ K, the high frequency limit has been measured at $T = 150$ K, i.e. at 18 K below T_g, where dipole motion is largely frozen and $\varepsilon' \approx \varepsilon_\infty$ at $\nu = 2$ kHz. In this situation, no second harmonic signal is detected at $E_p = 300$ kV cm^{-1} ($\varepsilon'_{E,2} = 5.6\times10^{-7} \pm 2.3\times10^{-4}$ across all five zones), see diamond in Fig. 5.

IV. DISCUSSION

In the series expansion for polarization at high fields E, $P = \varepsilon_0 \sum_{k=0}^{\infty} \chi_k E^k$, terms with even k are omitted for materials with inversion symmetry, such as most organic liquids. Examples for systems with susceptibilities χ_k of even order are electrets such as quartz and poled polymers with permanent or metastable polarization in the absence of an external field. These systems with non-vanishing χ_0 and χ_2 will generate second harmonic responses when subject to a sinusoidal field of sufficient magnitude. For the large class of materials with intrinsic inversion symmetry, i.e., with $\chi_2 = 0$, second harmonic generation (SHG) can be invoked by applying an external dc bias field. In these cases, the n^{th} harmonics of permittivity in the static limit can be related to χ_3 of Eq. (1) according to

$$\varepsilon_{E,1} - \varepsilon = \frac{3}{4}\chi_3 E_0^2 , \tag{3a}$$

$$\varepsilon_{E,2} = -\frac{6}{4}\chi_3 E_B E_0 , \tag{3b}$$

$$\varepsilon_{E,3} = -\frac{1}{4}\chi_3 E_0^2 , \tag{3c}$$

assuming that $\varepsilon_{E,n}$ is evaluated from an impedance measurement analogous to how ε is determined within the regime of linear response.[31]

For the particular case of PG, $\chi_3 = -2.3\times10^{-16}$ V^{-2} m^2 at $T = 225$ K has been determined consistently from both $\varepsilon_{E,1}$ and $\varepsilon_{E,3}$ data.[26] Note that this experimental approach to quantifying χ_3 did not involve the application of a dc bias field. According to theory,[31] the relation connecting χ_3 to the Piekara factor a is given by $a = (\varepsilon_{E,1} - \varepsilon)/E_B^2 = 3\chi_3$, with a being a commonly used gauge for the extent of nonlinear dielectric effects (NDE) in the static limit.[32] Therefore, Eq. (3b) provides a robust prediction for $\varepsilon_{E,2}$ at a given product of field amplitudes $E_B \times E_0$. For a given peak field $E_p = E_B + E_0$, the largest product $E_B \times E_0$ and thus $\varepsilon_{E,2}$ is achieved at $E_B = E_0$, the condition used to measure $\varepsilon_{E,2}$ in the static limit, see Fig. 1(a). The results of these experiments are compiled in Fig. 3 for three different peak fields E_p. The expectation based on the known value of χ_3 and Eq. (3b) is represented by solid line curves in Fig. 3. The field dependence of the measured $\varepsilon'_{E,2}$ levels shown in Fig. 3 is depicted more clearly as symbols versus the product $E_B \times E_0$ in Fig. 6, where the result for each zone is the average over eight out of ten periods, i.e., with the exception of the first and last period of a zone in which the E_B transitions occur. Apart from values taken at low field amplitudes, the $\varepsilon'_{E,2}$ results in Fig. 6 are near proportional to the product of ac

peak field times dc bias field, matching the slope $\partial\varepsilon_{E,2}/\partial(E_B E_0) = -1.5\chi_3$ of the dashed line predicted by Eq.(3b) better than the expectation that $\varepsilon'_{E,2} = 0$ when $E_B = 0$.

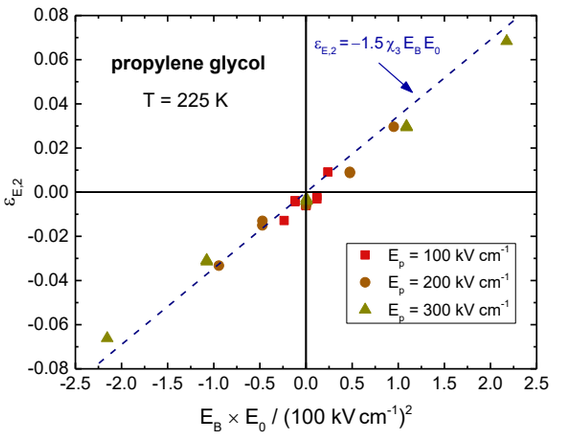

Fig. 6. Results for the field induced second harmonic permittivity in the static limit, $\varepsilon_{E,2}$, of PG at T = 225 K versus the product of the fields E_B and E_0. Each symbol represents the average over the respective zone shown in Fig. 3, using the same symbol shape and color. The dashed line shows the expected field dependence based on Eq. (3b) with $\chi_3 = -2.3\times10^{-16}$ V^{-2} m^2.

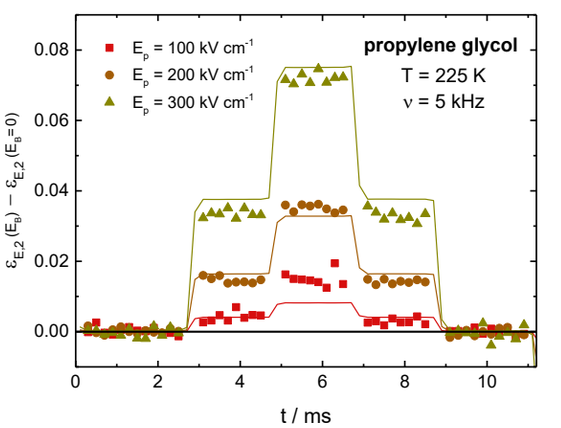

Fig. 7. Symbols represent results for the second harmonic high field permittivity in the static limit, $\varepsilon_{E,2}$, of PG at T = 225 K versus time, based on the data of zones 1 - 5 of Fig. 3, but shifted upward such that the average values of zones 1, 3, and 5 become zero for each E_p. Lines reflect the levels expected on the basis of the value for χ_3 for PG and Eq. (3b).

The relative discrepancies between experiment and theory are particularly significant at small fields, where $|\varepsilon'_{E,2}|$ remains below about 0.01, see Fig. 3 and Fig. 6. The main cause of this deviation is the second harmonic component $|E_2| \approx 10^{-3}|E_1|$ of the applied alternating field, resulting in a 10% and 30% uncertainty in $\varepsilon'_{E,2}$ at the highest and lowest fields, respectively. Therefore, the limited harmonic purity of the applied field explains the observed deviations seen in Fig. 3, which mainly amount to an offset $\varepsilon'_{E,2} < 0$ at $E_B = 0$. After offset correction, the agreement between experiment and the theoretical prediction of Eq. (3b) is improved, as shown for the first five zones in Fig. 7.

The present results of Fig. 4 and Fig. 5 reveal that second harmonic permittivities $\varepsilon'_{E,2}$ can not only be observed for low frequencies associated with responses in the static limit. In the situation leading to the results of Fig. 4, electronic polarizability and fast near-constant-loss modes contribute a considerable amount at the frequency $\nu = 2$ kHz at $T = 187$ K, where the peak loss frequency of PG is at $\nu_{max} = 74$ Hz and $\tau_{max} = 2.2$ ms. The overall amplitude of the second harmonic signal observed at frequencies $\nu = 10\,\nu_{max}$ in Fig. 4 is considerably below that seen in the static limit with $\nu = 0.008\,\nu_{max}$ in Fig. 3, and the $\varepsilon'_{E,2}$ data in each zone in Fig. 4(b) reaches a steady state level quickly relative to the α-relaxation time scale, indicated by the dashed line in Fig. 4(b). One possible explanation of the absence of a time dependence in the second harmonic permittivity observed at $30\,\nu_{max}$ is that electronic polarizability dominates in the generation of second harmonics in this case. To clarify whether electronic polarizability leads to second harmonics, we look at the frequency dependence of $\varepsilon'_{E,2}$ in Fig. 5, which demonstrates that $\varepsilon'_{E,2}(\omega)$ is reduced with increasing frequency in a manner proportional to $\varepsilon'(\omega) - \varepsilon_\infty$. In particular, no second harmonic signal could be detected in the high frequency limit, where dipolar contributions are absent and $\varepsilon' = \varepsilon_\infty$. Thus, an alternative explanation is required for not observing that the second harmonic signal appears as retarded in time as the polarization response, and perhaps instantaneously: When a dc bias electric field is applied in a step-like fashion, the orientation of molecules towards that field will be retarded according to the time scale of structural recovery (as in physical aging), which is governed by the structural or α-relaxation process.[33,34] However, the potential energy is tilted along the field direction as soon as the electric field is applied, thus creating an immediate loss of inversion symmetry, regardless of the more slowly changing state of polarization. Therefore, a near instantaneous appearance of SHG is a possibility.

In the present experiments, inversion symmetry has been broken by applying a dc bias field E_B, leading to measurable SHG signals. This implies that SHG can be detected by impedance spectroscopy also for materials with intrinsic anisotropy, either as bulk property or induced by interfaces, or by physical vapor deposition,[35,36] in which case no bias field is required. A classic example of exploiting SHG is measuring the return to the isotropic state of a previously poled polymer.[3,4] While the SHG of poled polymer has often been detected by optical techniques, the present experiments demonstrate that dielectric spectroscopy at twice the fundamental frequency is also capable of detecting anisotropy and its decay via structural relaxation to the isotropic state.

V. SUMMARY AND CONCLUSIONS

We have measured the second harmonic dielectric permittivity, $\varepsilon_{E,2}$, of propylene glycol (PG), with the inversion symmetry of the liquid broken by applying a dc bias electric field, E_B. The theoretical link between the third order susceptibility and the second harmonic permittivity $\varepsilon_{E,2} = -1.5\chi_3 E_B E_0$ has been verified in the static limit for the known value of χ_3 for PG and for different values of the peak ac field E_0 and dc bias field E_B. The amplitude of the second harmonic signal is observed to decrease with increasing temperature, and it also decreases with increasing frequency proportional to the real part of the relaxing low-field dielectric permittivity, i.e., $\varepsilon'_{E,2}(\omega) \propto \varepsilon'(\omega) - \varepsilon_\infty$. The present experiments also suggest that SHG can evolve faster than τ_α or even the instant a dc bias field is applied, rather than taking the α-relaxation time to approach its steady state level. However, more detailed experiments are required to confirm this notion.

We can conclude that this dielectric technique of detecting SHG is very sensitive to anisotropy, because in the present experiments $\mu E/k_B T$ remains below 6%, i.e., the degree of anisotropy induced by the present electric fields not exceeding 300 kV cm^{-1} is minimal. Therefore, dielectric spectroscopy with elevated ac field amplitudes (but without dc bias) can be employed to detect anisotropy that originates from previous poling, from interaction with interfaces, or from physical vapor deposition, to name a few examples.

ACKNOWLEDGMENTS

Insightful discussions with D. Matyushov are gratefully acknowledged. This research was supported by the National Science Foundation under grant number CHE-2153944.

AUTHOR DECLARATIONS

Conflict of Interest

The authors have no conflicts to disclose.

Author Contributions

Erik Thoms: Conceptualization (equal); Formal analysis (lead); Investigation (equal); Writing – review & editing (equal). **Ranko Richert:** Conceptualization (equal); Funding acquisition (lead); Investigation (equal); Writing – review & editing (equal).

DATA AVAILABILITY

The data that support the findings of this study are available from the corresponding author upon reasonable request.

REFERENCES

[1] P. N. Prasad and D. J. Williams, *Introduction to Nonlinear Optical Effects in Molecules and Polymers* (Wiley, New York, 1991).

[2] K. B. Eisenthal, "Liquid interfaces probed by second-harmonic and sum-frequency spectroscopy," Chem. Rev. **96**, 1343 (1996).

[3] K. D. Singer, J. E. Sohn, and S. J. Lalama, "Second harmonic generation in poled polymer films," Appl. Phys. Lett. **49**, 248 (1986).

[4] S. Schüssler, R. Richert, and H. Bässler, "Mechanisms of second harmonic generation efficiency relaxation in poled guest/host polymers," Macromol. **28**, 2429 (1995).

[5] P. Debye, *Polar Molecules* (Chemical Catalog Company, New York, 1929).

[6] A. Chełkowski, *Dielectric Physics* (Elsevier, Amsterdam, 1980).

[7] S. J. Rzoska and V. P. Zhelezny (Eds.), *Nonlinear Dielectric Phenomena in Complex Liquids* (Kluwer Academic Publishers, Dordrecht, 2004).

[8] R. Richert (Ed.), *Nonlinear Dielectric Spectroscopy* (Springer, Cham, 2018).

[9] R. Richert and S. Weinstein, "Nonlinear dielectric response and thermodynamic heterogeneity in liquids," Phys. Rev. Lett. **97**, 095703 (2006).

[10] W. Huang and R. Richert, "Dynamics of glass-forming liquids. XIII. Microwave heating in slow motion," J. Chem. Phys. **130**, 194509 (2009).

[11] C. Crauste-Thibierge, C. Brun, F. Ladieu, D. L'Hôte, G. Biroli, and J.-P. Bouchaud, "Evidence of growing spatial correlations at the glass transition from nonlinear response experiments," Phys. Rev. Lett. **104**, 165703 (2010).

[12] C. Brun, F. Ladieu, D. L'Hôte, M. Tarzia, G. Biroli, and J.-P. Bouchaud, "Nonlinear dielectric susceptibilities: Accurate determination of the growing correlation volume in a supercooled liquid," Phys. Rev. B **84**, 104204 (2011).

[13] Th. Bauer, P. Lunkenheimer, and A. Loidl, "Cooperativity and the freezing of molecular motion at the glass transition," Phys. Rev. Lett. **111**, 225702 (2013).

[14] D. L'Hôte, R. Tourbot, F. Ladieu, and P. Gadige, "Control parameter for the glass transition of glycerol evidenced by the static-field-induced nonlinear response," Phys. Rev. B **90**, 104202 (2014).

[15] S. Samanta and R. Richert, "Dynamics of glass-forming liquids. XVIII. Does entropy control structural relaxation times?," J. Chem. Phys. **142**, 044504 (2015).

[16] A. R. Young-Gonzales, S. Samanta, and R. Richert, "Dynamics of glass-forming liquids. XIX. Rise and decay of field induced anisotropy in the non-linear regime," J. Chem. Phys. **143**, 104504 (2015).

[17] P. Kim, A. R. Young-Gonzales, and R. Richert, "Dynamics of glass-forming liquids. XX. Third harmonic experiments of non-linear dielectric effects versus a phenomenological model," J. Chem. Phys. **145**, 064510 (2016).

[18] S. Albert, Th. Bauer, M. Michl, G. Biroli, J.-P. Bouchaud, A. Loidl, P. Lunkenheimer, R. Tourbot, C. Wiertel-Gasquet, and F. Ladieu, "Fifth-order susceptibility unveils growth of thermodynamic amorphous order in glass-formers," Science **352**, 1308 (2016).

[19] R. Richert, "Nonlinear dielectric effects in liquids: A guided tour," J. Phys.: Condens. Matter **29**, 363001 (2017).

[20] R. Richert, "Perspective: Nonlinear approaches to structure and dynamics of soft materials," J. Chem. Phys. **149**, 240901 (2018).

[21] J. L. Déjardin and Y. P. Kalmykov, "Nonlinear dielectric relaxation of polar molecules in a strong ac electric field: Steady state response," Phys. Rev. E **61**, 1211 (2000).

[22] L. Berthier, G. Biroli, J.-P. Bouchaud, L. Cipelletti, D. El Masri, D. L'Hôte, F. Ladieu, and M. Pierno, "Direct experimental evidence of a growing length scale accompanying the glass transition," Science **310**, 1797 (2005).

[23] D. V. Matyushov, "Nonlinear dielectric response of polar liquids," J. Chem. Phys. **142**, 244502 (2015).

[24] M. Hénot and F. Ladieu, "Emergence of a hump in the cubic dielectric response of glycerol," Phys. Rev. Lett. **134**, 218202 (2025).

[25] K. Adrjanowicz, M. Paluch, and R. Richert, "Formation of new polymorphs and control of crystallization in molecular glass-formers by electric field," Phys. Chem. Chem. Phys. **20**, 925 (2018).

[26] E. Thoms and R. Richert, "New experimental approach to nonlinear dielectric effects in the static limit," J. Mol. Liquids **340**, 117107 (2021).

[27] C. Deng and K. Zhang, "Thermal conductivity of 1,2-ethanediol and 1,2-propanediol binary aqueous solutions at temperature from 253 K to 373 K," Int. J. Thermophys. **42**, 81 (2021).

[28] D. W. Davidson and R. H. Cole, "Dielectric relaxation in glycerol, propylene glycol, and n-propanol," J. Chem. Phys. **19**, 1484 (1951).

[29] S. Weinstein and R. Richert, "Nonlinear features in the dielectric behavior of propylene glycol," Phys. Rev. B **75**, 064302 (2007).

[30] Th. Bauer, M. Michl, P. Lunkenheimer, and A. Loidl, "Nonlinear dielectric response of Debye, α, and β relaxation in 1-propanol," J. Non-Cryst. Solids **407**, 66 (2015).

[31] R. Richert and D. V. Matyushov, "Quantifying dielectric permittivities in the nonlinear regime," J. Phys. Condens. Matter **33**, 385101 (2021).

[32] Y. Marcus and G. Hefter, "On the pressure and electric field dependencies of the relative permittivity of liquids," J. Solution Chem. **28**, 575 (1999).

[33] R. Richert, J. P. Gabriel, and E. Thoms, "Structural relaxation and recovery: A dielectric approach," J. Phys. Chem. Lett. **12**, 8465 (2021).

[34] J. P. Gabriel and R. Richert, "Comparing two sources of physical aging: Temperature vs electric field," J. Chem. Phys. **159**, 164502 (2023).

[35] M. D. Ediger, J. de Pablo, and L. Yu, "Anisotropic vapor-deposited glasses: Hybrid organic solids," Acc. Chem. Res. **52**, 407 (2019).

[36] P. Luo and Z. Fakhraai, "Surface-mediated formation of stable glasses," Annu. Rev. Phys. Chem. **74**, 361 (2023).